Coherent algorithm for detection of gravitational wave bursts

S. Klimenko, I. Yakushin†, A. Mercer, G. Mitselmakher

University of Florida, P.O.Box 118440, Gainesville, Florida, 32611, USA †LIGO Livingston observatory, P.O. Box 940, Livingston, Luisiana, 70754, USA

LIGO-P070093-00-Z

Abstract. We describe a coherent network algorithm for detection and reconstruction of gravitational wave bursts. The algorithm works for two and more arbitrary aligned detectors and can be used both for all-sky and triggered burst searches. We discribe the main components of the algorithm, including the time-frequency analysis in wavelet domain, cohstruction of the likelihood time-frequency maps, the generation and selection of the burst events.

1. Introduction

Coherent network analysis is addressing a problem of detection and reconstruction of gravitational waves with the networks of GW detectors. It has been extensively studied in the literature [1, 2, 3, 4, 5, 6] in application to detection of the bursts signals, which may be produced by numerous gravitational wave sources in the Universe [7, 8, 9, 10, 11, 12, 13, 14, 15]. In the coherent methods, a statistic is built as a coherent sum over detector responses and, in general, it is expected to be more optimal (better sensitivity at the same false alarm rate) than the detection statistics of individual detectors. Also coherent methods provide estimators for the GW waveforms and the source coordinates in the sky.

The method we present (called coherent WaveBurst) is significantly different from the traditional burst detection methods. Unlike the coincident methods [16, 17, 18], which first identify gravitational wave events in individual detectors by using excess power statistic and than require coincidence between the detectors, the coherent WaveBurst combines all data streams into one coherent statistic constructed in the framework of the constrained maximum likelihood analysis [4]. Such approach has significant advantages over the coincident methods. First, the sensitivity of the method is not limited by the least sensitive detector in the network. The detection is based on the coherent statistic which represents the total signal-to-noise ratio of the GW signal detected in the network. Second, other coherent statistics, such as the null stream and the network correlation coefficient can be constructed to distinguish genuine GW signals from the environmental and instrumental artefacts. Finally, the source coordinates of the GW waveforms can be reconstructed.

2. Coherent analysis

The coherent WaveBurst pipeline uses a method for a coherent detection and reconstruction of burst signals based on the use of the likelihood ratio functional [4]. For a general case of Gaussian quasi-stationary noise it can be written in the wavelet (time-frequency) domain as

$$\mathcal{L} = \sum_{k=1}^{K} \sum_{i,j=1}^{N} \left(\frac{w_k^2[i,j]}{\sigma_k^2[i,j]} - \frac{(w_k[i,j] - \xi_k[i,j])^2}{\sigma_k^2[i,j]} \right) , \tag{1}$$

where K is the number of detectors in the network, $w_k[i,j]$ is the sampled detector data (time i and frequency j indexes run over some TF area of size N) and $\xi_k[i,j]$ are the detector responses. Note, we omit a traditional term $1/2$ in the definition of the likelihood ratio. The detector noise is characterized by its standard deviation $\sigma_k[i,j]$, which may vary over the TF plane. The detector responses are written in the standard notations

$$\xi_k[i,j] = F_{+k}h_+[i,j] + F_{\times k}h_\times[i,j] , \tag{2}$$

where $F_{+k}(\theta,\phi)$, $F_{\times k}(\theta,\phi)$ are the detector antenna patterns (depend upon source coordinates θ and ϕ) and $h_+[i,j]$, $h_\times[i,j]$ are the two polarizations of the gravitational wave signal in the wave frame. Since the detector responses ξ_k are invariant with respect to the rotation around z-axis in the wave frame, the polarization angle is included in the definition of the h_+ and $h_\times$. The GW waveforms h_+ and $h_\times$ are found by variation of $\mathcal{L}$. The maximum likelihood ratio is obtained by substituting the solutions into the functional $\mathcal{L}$. The waveforms in time domain are reconstructed from the inverse wavelet transformation. Below, for convenience we introduce the data vector $\mathbf{w}[i,j]$ and the antenna pattern vectors $\mathbf{f}_+[i,j]$ and $\mathbf{f}_\times[i,j]$

$$\mathbf{w}[i,j] = \left(\frac{w_1[i,j]}{\sigma_1[i,j]}, ..., \frac{w_K[i,j]}{\sigma_K[i,j]} \right) \tag{3}$$

$$\mathbf{f}_{+(\times)}[i,j] = \left(\frac{F_{1+(\times)}}{\sigma_1[i,j]}, ..., \frac{F_{K+(\times)}}{\sigma_K[i,j]} \right) \tag{4}$$

Further in the text we omit the time-frequency indexes and replace the sum $\sum_{i,j=1}^{N}$ with $\sum_{\Omega_{TF}}$, where Ω_{TF} is the time-frequency area selected for the analysis.

The likelihood functional (Eq.1) can be written in the form $\mathcal{L} = \mathcal{L}_1 + \mathcal{L}_2$:

$$\mathcal{L}_+ = \sum_{\Omega_{TF}} \left[(\mathbf{w} \cdot \mathbf{f}_+)h_+ - \frac{1}{2}|\mathbf{f}_+|^2 h_+^2 \right] , \tag{5}$$

$$\mathcal{L}_\times = \sum_{\Omega_{TF}} \left[(\mathbf{w} \cdot \mathbf{f}_\times)h_\times - \frac{1}{2}|\mathbf{f}_\times|^2 h_\times^2 \right] , \tag{6}$$

where the antenna pattern vectors $\mathbf{f}_+$ and $\mathbf{f}_\times$ are defined in the Dominant Polarization wave Frame (DPF) [4]. In this frame the antenna pattern vectors are orthogonal to each other: $(\mathbf{f}_+ \cdot \mathbf{f}_\times) = \mathbf{0}$. The estimators of the GW waveforms are the solutions of the

equations

$$(\mathbf{w} \cdot \mathbf{f}_+) = |\mathbf{f}_+|^2 h_+ \; , \tag{7}$$

$$(\mathbf{w} \cdot \mathbf{f}_\times) = |\mathbf{f}_\times|^2 h_\times \; . \tag{8}$$

Note, the norm of $|\mathbf{f}_+|^2$ and $|\mathbf{f}_\times|^2$ characterize the network sensitivity to the h_+ and $h_\times$ polarizations.

2.1. Likelihood regulators

As first shown in [4], there is a specific class of constraints (often called regulators), which arise from the way the network responds to a generic gravitational wave signal. A classical example is a network of aligned detectors where the detector responses ξ_k are identical. Therefore the algorithm can be constrained to search for an unknown function ξ rather than for two gravitational wave polarizations h_+ and $h_\times$, which span much larger parameter space. Note, in this case $|\mathbf{f}_\times|^2 = 0$, the Equation 8 is ill-conditioned and the solution for the $h_\times$ waveform can not be found. The regulators are important not only for aligned detectors, but also for networks of miss-aligned detectors, for example, the LIGO and Virgo network [20, 21]. Depending on the source location the network can be much less sensitive to the second GW component ($|\mathbf{f}_\times|^2 << |\mathbf{f}_+|^2$) and the $h_\times$ waveform may not be reconstructed from noisy data.

In the coherent WaveBurst analysis we introduce a regulator by changing the norm of the $\mathbf{f}_\times$ vector

$$|\mathbf{f}'_\times|^2 = |\mathbf{f}_\times|^2 + \delta, \tag{9}$$

where δ is some parameter. This is equivalent to adding one more, dummy detector, to the network with the antenna patterns $f_{+,K+1} = 0$, $f_{\times,K+1} = \sqrt{\delta}$ and zero detector output ($x_{K+1} = 0$). In this case, the regulator preserves the orthogonality of the vectors $\mathbf{f}_+$ and $\mathbf{f}'_\times$ and the maximum likelihood statistic is written as

$$L_{max} = \sum_{\Omega_{TF}} \left[\frac{(\mathbf{w} \cdot \mathbf{f}_+)^2}{|\mathbf{f}_+|^2} + \frac{(\mathbf{w} \cdot \mathbf{f}'_\times)^2}{|\mathbf{f}'_\times|^2} \right] = \sum_{\Omega_{TF}} \left[(\mathbf{w} \cdot \mathbf{e}_+)^2 + (\mathbf{w} \cdot \mathbf{e}'_\times)^2 \right], \tag{10}$$

where $\mathbf{e}_+$ and $\mathbf{e}'_\times$ are unity vectors. Depending on the value of the parameter δ different statistics can be generated, for example:

- $\delta = 0$ - standard likelihood,
- $\delta = \infty$ - hard constraint likelihood.

2.2. Reconstruction of GW waveforms

The GW waveforms are given by the solutions of the likelihood functional Eq.5,6. For the first GW component the solution is

$$h_+ = \frac{(\mathbf{w} \cdot \mathbf{f}_+)}{|\mathbf{f}_+|^2}. \tag{11}$$

When the regulator is introduced it affects the solution for the second GW component. In this case we look for such a solution, which gives the second term of the likelihood statistic L_{max}, when the solution is substituted into the likelihood functional. Namely, we solve the equation

$$2(\mathbf{w} \cdot \mathbf{f}_\times)h_\times - |\mathbf{f}_\times|^2 h_\times^2 - \frac{(\mathbf{w} \cdot \mathbf{f}'_\times)^2}{|\mathbf{f}'_\times|^2} = 0. \tag{12}$$

Out of two possible solutions the following one is selected

$$h_\times = \frac{(\mathbf{w} \cdot \mathbf{f}_\times)}{|\mathbf{f}'_\times|^2} \left(1 + \sqrt{1 - \frac{|\mathbf{f}_\times|^2}{|\mathbf{f}'_\times|^2}}\right)^{-1}. \tag{13}$$

In case of aligned detectors ($|f_\times| = 0$) this equation results in a trivial solution $h_\times = 0$.

3. Data analysis algorithms

In this section we describe the algorithms used in the coherent WaveBurst pipeline. They include: wavelet transformation, conditioning of input data, construction of time delay filters and generation of coherent triggers.

3.1. Wavelet transformation

The discrete wavelet transformations (DWT) are applied to discrete data and produce discrete wavelet series $w[ij]$, where j is the scale index (dilation) and i is a time index (translation). Applied to time series, the DWT maps data from time domain to wavelet domain. All DWTs used in cWB have *critical sampling* when the output data vector has the same size as the input data vector.

Wavelet series give a time-scale representation of data where each wavelet scale can be associated with a certain frequency band of the initial time series. Therefore the wavelet time-scale spectra can be displayed as a time-frequency scallogram, where the scale is replaced with the central frequency f of the band. The time series sampling rate R and the scale number j determine the time resolution $\Delta t_j(R)$ at this scale. The DWT preserves the time-frequency volume of the data samples, which is equal to $1/2$ for the input time series. Therefore the frequency resolution Δf_j is defined as $1/(2\Delta t_j)$ and determines the data bandwidth at the scale j. For optimal localization of the GW energy on the TF plane, the cWB analysis is performed at several time-frequency resolutions.

The time-frequency resolution defined above should be distinguished from the intrinsic TF resolution of the wavelet transformation, which defines the spectral leakage between the wavelet sub-bands and depends on the length of the wavelet filter. To reduce spectral leakage we use Meyers wavelets for which long filters can be easily constructed [22]. As shown in Figure 1, it allows us much better localization of the burst energy on the time-frequency plane than for the Symlet60 wavelets used for the LIGO S2-S4 analysis [23, 24]. The disadvantage of the Meyer filters is that for the local support they have to be trancated. As the result, the Meyer wavelets are approximately orthonormal.
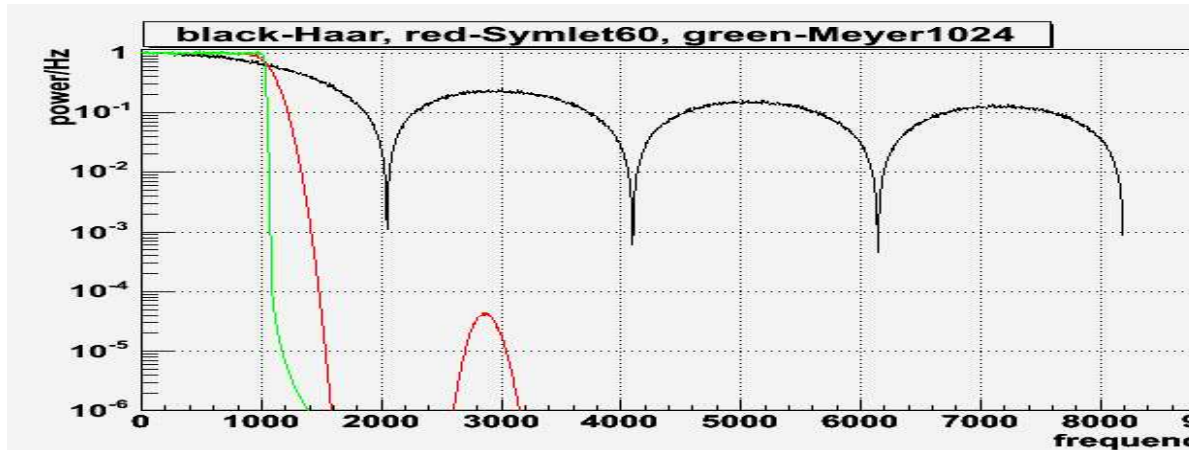
Figure 1. Comparison of spectral leakage from the first (low) frequency band to the high frequency bands for Haar, Symlet_60 and Meyer_1024 wavelets after three wavelet decomposition steps.

From the other side the Meyer filters can be constructed so that the Parseval identity holds with better then 0.01% accuracy, which is more than adequate for the analysis.

3.2. Linear prediction error filter

The linear prediction error (LPE) filters are used to remove "predictable" components from an input time series. Usually they are constructed and applied in time domain. In this case the output of the LPE filter is a whitened time series. The LPE filters can be also used in the wavelet domain. For construction of the LPE filters we follow the approach described in [26] The symmetric LPE filters can be constructed from the backward and forward LPE filters by using classical Levinson algorithm or the split lattice algorithm.

Since each wavelet layer is a time series, rather than applying LPE filter to a time series $x(t)$, one can perform a wavelet decomposition $x(t) \rightarrow w(f,t)$ first, and than construct and apply the LPE filter $F(f)$ individually to each wavelet layer. A set of filters $F(f)$ remove predictable components (like lines) in the wavelet layers producing data $w'(t)$. The filtered time series $x'(t)$ can be reconstructed from $w'(t)$. An example PSD of the filtered S4 data is shown in Figure 2. As one can see, when applied in wavelet domain the LPE filter removes data artifacts but preserves the power spectral
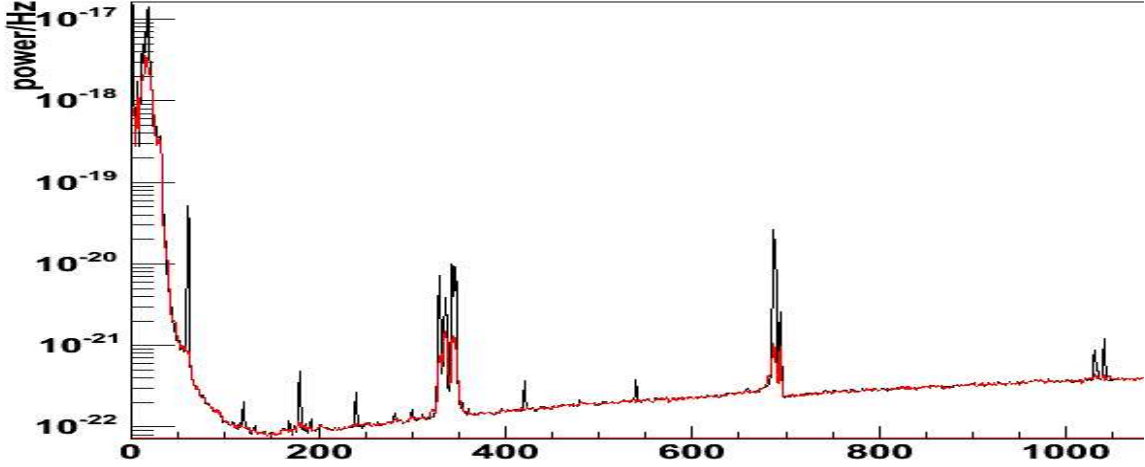
density of the noise floor.

Figure 2. Power spectra of original (black) and LPE filtered (red) noise of the Hanford 4k detector.

3.3. Time delay filters in wavelet domain

The likelihood method requires calculation of the inner products $\langle x_n(\tau_n), x_m(\tau_m) \rangle$, where the data streams are shifted in time to take into account the GW signal time delay between the detectors n and m. The time delay $\tau_n - \tau_m$ in turn, depends on the source coordinates θ and ϕ.

In time domain it is straightforward to account for the time delays. But for colored detector noise it is preferable to calculate the maximum likelihood statistics in the Fourier or wavelet (time-frequency) domains. In the wavelet domain one needs to calculate the inner products $\langle w_n(\tau_n), w_m(\tau_m) \rangle$. The delayed amplitudes can be calculated from the original amplitudes (before delay) with the help of the time delay filter $D_{kl}(\tau)$

$$w_{n,m}(i, j, \tau) = \sum_{kl} D_{kl}(\tau, j) w_{n,m}(i + k, j + l), \tag{14}$$

where k and l are the local TF coordinates with respect to the TF location (i,j). The delay filters are constructed individually for each wavelet layer, which is indicated with the index j.

The construction of the delay filters is related to the decomposition of the sampled wavelet functions $\Psi_j(t+\tau)$ in the basis of the non-shifted wavelet functions $\Psi_j(t)$. The delay filter construction procedure can be described in the following steps:

- create a wavelet series with only one coefficient at the TF location (i,j) set to unity,
- apply the inverse wavelet transformation reconstructing $\Psi_j(t)$ in time domain,
- shift $\Psi_j(t)$ by delay time τ and perform wavelet decomposition of $\Psi_j(t+\tau)$,
- the resulting wavelet amplitudes at the TF locations $(i+k, j+l)$ give the delay filter coefficients $D_{kl}(\tau, j)$ for the wavelet layer j.

The length of the delay filter is determined by the requirement on the acceptable energy loss when the delay filter is applied. By sorting D_{kl}^2 in the decreasing order the fractional energy loss is

$$\epsilon_K = 1 - \sum_K D_{kl}^2, \tag{15}$$

where the sum is calculated over K most significant coefficients. The selected coefficients are also described by the list of their relative TF locations (k, l) which should be stored along with the filter coefficients D_{kl}. Typically K should be greater then 20 to obtain the fractional energy loss less than 1%.

3.4. Generation of coherent triggers

A starting point of any burst analysis is the identification of burst events (triggers). Respectively, this stage of a burst analysis pipeline is called the event trigger generator (ETG). Usually, the ETGs based on the excess power statistics of individual detectors are used in the analysis [16, 17, 18]. Another example of ETG is corrPower algorithm [19], which uses cross-correlation between detector pairs to generate the triggers. The likelihood statistic used in the coherent WaveBurst utilizes both the excess power and the cross-correlation terms.

3.4.1. Likelihood time-frequency map In general the likelihood functional is calculated as a sum over the data samples selected for the analysis (see Eq.1). The number of terms in the sum depends on the selected TF area in the wavelet domain. When the sum consists of only one term, one can write the likelihood functional for a given TF location and point in the sky ‡:

$$\mathcal{L}_p(i, j, \theta, \phi) = |\mathbf{w}|^2 - |\mathbf{w} - \mathbf{f}_+ h_1 - \mathbf{f}_\times h_2|^2. \tag{16}$$

Since the entire likelihood approach is applicable to the functional above, one can solve the variation problem and find the maximum likelihood statistics $L_p(\theta, \phi)$. They can be maximized over the source coordinates θ and ϕ, resulting in the statistics

$$L_m(i, j) = max_{\theta, \phi}\{L_p(i, j, \theta, \phi)\}. \tag{17}$$

Calculated as a function of time and frequency, it gives us a likelihood time-frequency (LTF) map. Figure 3 shows an example of the LTF map for a segment of the S4 data.

‡ For definition of vectors $\mathbf{w}$, $\mathbf{f}_+$, and $\mathbf{f}_\times$ see Eq.3,4
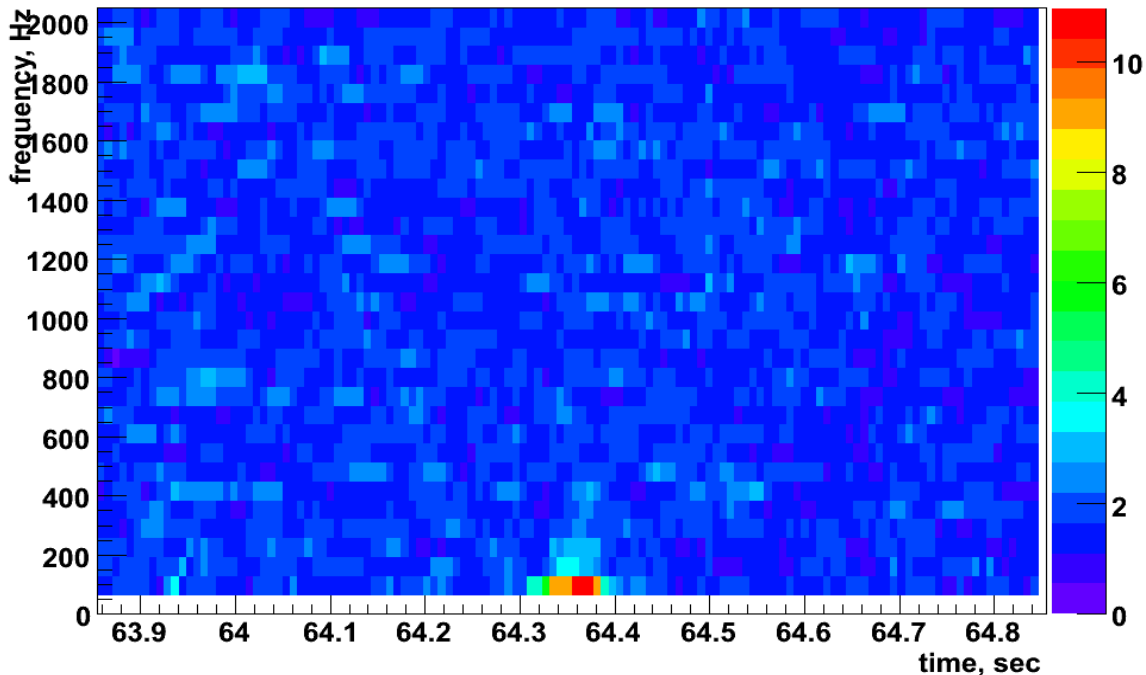
Figure 3. Example of the LTF map for a magnetic glitch in S4 L1xH1xH2 data.

A single data sample in the map is called the LTF pixel. It is characterized by its TF location (i,j) and by the wavelet amplitudes $w_k(i, j, \tau_k(\theta, \phi))$, which are used to construct the likelihood statistics L_p.

3.4.2. Coherent triggers The statistic L_m has a meaning of the maximum possible energy detected by the network at a given TF location. By selecting the values of L_m above some threshold, one can identify groups of the LTF pixels (coherent trigger) on the time-frequency plane. A coherent trigger is defined for the entire network, rather than for individual detectors. Therefore, further in the text we reserve a name "cluster" for a group of pixels selected in a single detector and refer to a group of the LTF pixels as a coherent or network trigger.

After the coherent triggers are identified, one has to reconstruct the parameters of the GW bursts associated with the triggers, including the reconstruction of the source coordinates, the two GW polarizations, the individual detector responses and the maximum likelihood statistics of the triggers. The likelihood of reconstructed triggers is calculated as

$$\mathcal{L}_c(\theta, \phi) = \sum_{ij} \mathcal{L}_p(i, j, \theta, \phi) \qquad (18)$$

where the sum is taken over the LTF pixels in the trigger. The maximum likelihood statistic L_{max} is obtained by variation of L_c over θ and ϕ. Unlike for L_p, which is

calculated for a single LTF pixel, the L_{max} is calculated simultaneously for all LTF pixels forming the coherent trigger.

4. Coherent statistics

When the detector noise is Gaussian and stationary, the maximum likelihood L_{max} is the only statistic required for detection and selection of the GW events. In this case the pipeline false alarm and false dismissal probabilities are controlled by the threshold on L_{max}. The real data, however, is contaminated with the instrumental and environmental glitches and additional selection cuts should be applied to distinguish genuine GW signals [25, 6]. Such selection cuts test the consistency of the reconstructed responses in the detectors. In the coherent WaveBurst method the consistency test is based on the coherent statistics constructed from the elements of the likelihood and the null matrices.

The likelihood matrix L_{nm} is obtained from the likelihood quadratic form (see Eq.19)

$$L_{max} = \sum_{nm} L_{nm} = \sum_{nm} \left[\langle w_n w_m e_{+n} e_{+m} \rangle + \langle w_n w_m e'_{\times n} e'_{\times m} \rangle \right]. \tag{19}$$

The diagonal (off-diagonal) terms of the matrix L_{mn} describe the reconstructed normalized incoherent (coherent) energy. The sum of the off-diagonal terms is the coherent energy E_{coh} detected by the network. The coherent terms can also be used to construct the correlation coefficients:

$$r_{nm} = \frac{L_{nm}}{\sqrt{L_{nn}L_{mm}}}. \tag{20}$$

which represent Pearson's correlation coefficients in the case of aligned detectors. We use the coefficients r_{nm} to construct the reduced coherent energy

$$e_{coh} = \sum_{nm} L_{nm}|r_{nm}|. \tag{21}$$

which provides one of the most efficient selection cuts for rejection of the incoherent background events.

The null matrix represents the normalized energy of the reconstructed detector noise

$$N_{nm} = E_{nm} - L_{nm}, \tag{22}$$

where E_{nm} is the diagonal matrix of the normalized energy in the detectors: $E_{nn} = \langle x_n^2 \rangle$. To distinguish genuine GW signals from the instrumental and invironmental glitches we introduce the network correlation coefficients

$$C_{net} = \frac{E_{coh}}{N + |E_{coh}|}, \quad c_{net} = \frac{e_{coh}}{N + |e_{coh}|} \tag{23}$$

where N is a sum of all elements of the null matrix. Usually for glitches little coherent energy is detected and the reconstructed detector responses are inconsistent with the detector outputs which results in the large null energy. Therefore the correlation coefficients C_{net} and c_{net} can be used for a veto cut which effectively compares the null

energy with the coherent energy. This is much safer veto than the null stream veto [25] where the null energy is compared with the estimated noise energy. In any realistic data analysis there is always some residual energy left in the null stream. Therefore for strong gravitational waves the energy of the residual signal can be much larger than the noise energy resulting in false rejection of the GW signal. This is not the case for the veto cut based on C_{net} and c_{net}.

5. Summary

In the paper we discussed how the coherent network algorithms are constructed for burst searches. We found it convenient to construct coherent burst searches in the time-frequency (wavelet) domain, which requires construction of the time delay filters. For detection of burst signals we combine output of all detectors into one coherent statistic - likelihood, which represents the total signal-to-noise ratio of the signal detected by the network. To distinguish genuine GW signals from the instrumental and invironmental glitches we introduced several coherent statistics constructed from the elements of the likelihood and null matrix. We do not discuss the performance of the method in this paper. However, we did numerous studies of the method with different sets of the real LIGO and Vergo data. We found that, in general, the method has better performance than the burst algorithm used for the analysis of LIGO data [16, 20, 21]. The results of this of these studies will be presented in the subsequent papers.

6. Acknowledgments

7. References

 [1] Y. Gursel and M. Tinto, Phys. Rev. D **40**, 3884 (1989)
 [2] E. E. Flanagan and S. A. Hughes, Phys. Rev. D **57**, 4577 (1998)
 [3] N. Arnaud et al, Phys. Rev. D **68**, 102001 (2003)
 [4] S.Klimenko, S.Mohanty, M.Rakhmanov, G.Mitselmakher, Phys. Rev. D **72**, 122002 (2005).
 [5] M. Rakhmanov *Class. Quantum Grav.* **23** S673 (2006)
 [6] S. Chatterji et al, Phys.Rev. D **74** 082005 (2006)
 [7] T. Zwerger and E. Mueller, Astron. Astrophys, 320, 209 (1997)
 [8] H. Dimmelmeier, J. A. Font and E. Mueller, Astron. Astrophys, 393, 523 (2002)
 [9] C. Ott et al, Astrophys. J., 600, 834 (2004)
[10] M. Shibata and Y. I. Sekiguchi, Phys. Rev. D **69**, 084024 (2004)
[11] E. E. Flanagan and S. A. Hughes, Phys. Rev. D **57**, 4535 (1998)
[12] J. Baker et al, Phys. Rev. D **73**, 104002 (2006)
[13] F. Pretorius, Phys. Rev. Lett. **95**, 121101 (2005)
[14] M. Campanelli et al, Phys. Rev. Lett. **96**, 111101 (2006)

[15] P. Meszaros, Rept. Prog. Phys. 69, 2259-2322 (2006)

[16] S. Klimenko and G. Mitselmakher, Wavelet method for GW burst detection *Class. Quantum Grav.* **21**, S1819 (2004). *Class. Quantum Grav.* **21**, S1685 (2004).

[17] S. Chatterji, L. Blackburn, G. Martin, E. Katsavounidis, Multiresolution techniques for the detection of gravitational-wave bursts. Class. Quantum Grav. **21**, S1809 (2004).

[18] J.W.C. McNabb et al, arXiv:gr-qc/0404123 v1 29, April 2004

[19] L. Cadonati, Coherent waveform consistency test for LIGO burst candidates. *Class. Quantum Grav.* **21**, S1695 (2004).

[20] B. Abbott et al, (The LIGO Scientific Collaboration), *Class. Quantum Grav.* **23**, S51-S56 (2006)

[21] F. Acernese et al, (The Virgo Collaboration), *Class. Quantum Grav.* **23**, S63-S69 (2006)

[22] B. Vidakovic, Statistical modeling by wavelets, 1999.

[23] B. Abbot et al, Phys. Rev. D **72**, (2005) 062001

[24] B. Abbot et al, *Class. Quantum Grav.* **24** 5343-5369 (2007)

[25] L. Wen and B. F. Schutz,Coherent network detection of gravitational waves: the redundancy veto, Class. Quantum Grav. **22**, S1321 (2005).

[26] P. Delsarte and Y. Genin, On the Splitting of classical algorithms in Linear prediction theory, IEEE, ASSP-35, 1987